NANO LETTERS

LETTER

pubs.acs.org/NanoLett

$In_xGa_{1-x}As$ Nanowires on Silicon: One-Dimensional Heterogeneous Epitaxy, Bandgap Engineering, and Photovoltaics

Jae Cheol Shin,[†] Kyou Hyun Kim,[‡] Ki Jun Yu,[†] Hefei Hu,[‡] Leijun Yin,[§] Cun-Zheng Ning,[§] John A. Rogers,[‡,†] Jian-Min Zuo,[‡] and Xiuling Li[*,†,‡]

[†]Department of Electrical and Computer Engineering, [‡]Department of Materials Science and Engineering, University of Illinois, Urbana, Illinois 61801, United States

[§]School of Electrical, Computer and Energy Engineering, Arizona State University, Tempe, Arizona 85287, United States

Supporting Information

ABSTRACT: We report on the one-dimensional (1D) heteroepitaxial growth of $In_xGa_{1-x}As$ ($x = 0.2-1$) nanowires (NWs) on silicon (Si) substrates over almost the entire composition range using metalorganic chemical vapor deposition (MOCVD) without catalysts or masks. The epitaxial growth takes place spontaneously producing uniform, nontapered, high aspect ratio NW arrays with a density exceeding $1 \times 10^8/cm^2$. NW diameter (~30−250 nm) is inversely proportional to the lattice mismatch between $In_xGa_{1-x}As$ and Si (~4−11%), and can be further tuned by MOCVD growth condition. Remarkably, no dislocations have been found in all composition $In_xGa_{1-x}As$ NWs, even though massive stacking faults and twin planes are present. Indium rich NWs show more zinc-blende and Ga-rich NWs exhibit dominantly wurtzite polytype, as confirmed by scanning transmission electron microscopy (STEM) and photoluminescence spectra. Solar cells fabricated using an n-type $In_{0.3}Ga_{0.7}As$ NW array on a p-type Si(111) substrate with a ~2.2% area coverage, operates at an open circuit voltage, V_{oc}, and a short circuit current density, J_{sc}, of 0.37 V and 12.9 mA/cm^2, respectively. This work represents the first systematic report on direct 1D heteroepitaxy of ternary $In_xGa_{1-x}As$ NWs on silicon substrate in a wide composition/bandgap range that can be used for wafer-scale monolithic heterogeneous integration for high performance photovoltaics.

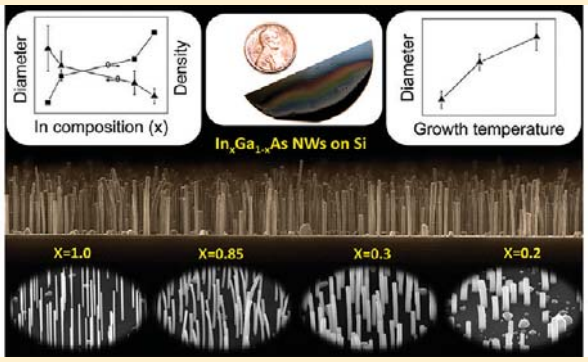

KEYWORDS: Nanowire, solar cell, heterogeneous integration, III-V on Si, InGaAs nanowire, InAs nanowire

Heterogeneous integration of III−V compound semiconductor and silicon (Si) has been researched for many years since Si is the prevalent platform for microelectronics while III−V can be used for optoelectronics due to its direct bandgap and versatile heterojunctions.[1−3] To increase the functionality of III−V devices on Si, it is essential to be able to engineer the bandgap in a wide range. For thin films, lattice mismatch is the formidable limitation preventing defect-free monolithic heteroepitaxy of III-Vs on Si over a wide range of compositions hence bandgaps. One-dimensional (1D) heteroepitaxy on the other hand can accommodate mismatch strain through lateral strain relaxation, allowing nanowires (NWs) epitaxially grown on substrates with as much as 46% lattice mismatch.[3−9] Direct growth of NW arrays without a catalyst is of particular interest due to its simplicity in processing as well as the metal-free environment, since potential incorporation of deep levels from metal catalysts such as Au used in vapor-liquid-solid (VLS) growth is a big concern.[10,11] For this reason, direct growth mechanism of InAs NWs on Si surface has been studied in the past several years[12−15] and devices including wrap-around gate transistors, photodetectors, and solar cells have been demonstrated using InAs NW array on Si.[5,16,17] However, the bandgap of InAs is relatively small (0.36 eV) and this causes low on−off ratio for electrical devices and low open circuit voltage and limited absorption range for photovoltaic devices.[5,16] Bandgap engineering of NWs on Si platform has enabled high-performance electronic and photonic devices over a variety of wavelength range.[18−23] So far, most reports of III−V NWs on Si have been focused on binary semiconductors, including InAs and InP. Direct heteroepitaxial growth of $In_xGa_{1-x}As$ NW on Si allows the tuning of bandgap in a wide wavelength range in the near IR from ~870−3500 nm. The most recent demonstration of an optically pumped nanolaser, consisting of a single $In_xGa_{1-x}As$ ($x = 0.15-0.2$) tapered nanocone on roughened silicon(111) substrate,[24,25] underlines the importance of ternary $In_xGa_{1-x}As$ 1D structures. However, the density of these nanocones appears to be quite low ($\sim 5 \times 10^5/cm^2$) and the height seems to be limited by the cone tapering angle, which present challenges for array based NW applications such as solar cells. Composition range beyond $x = 0.2$ remains unexplored and not much structural analysis has been reported to guide the 1D heteroepitaxy of

Received: August 3, 2011
Revised: September 29, 2011
Published: October 03, 2011

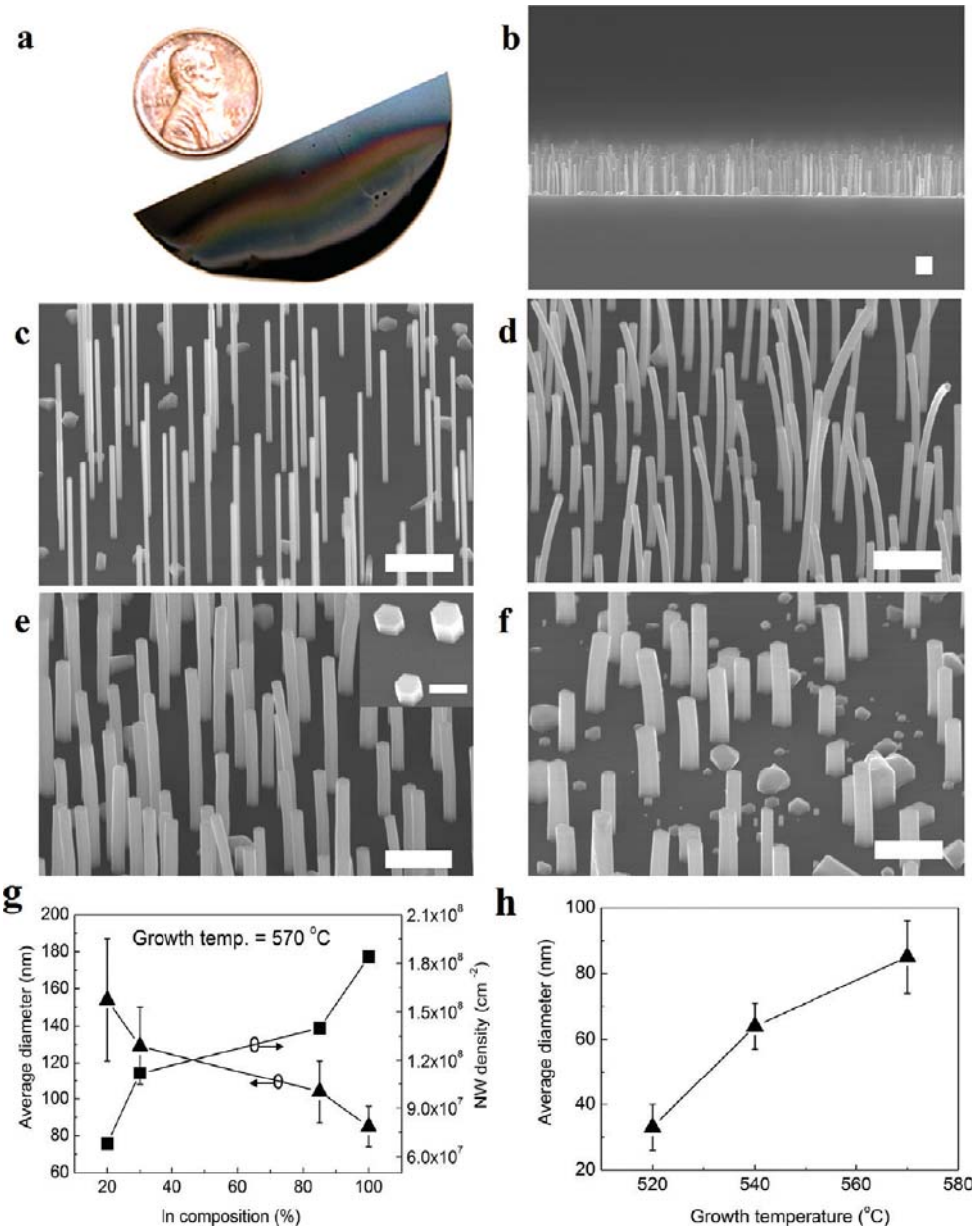

Figure 1. Optical and SEM images of $In_xGa_{1-x}As$ NWs on Si(111) substrates, and diameter and density dependence on NW composition and growth temperature. (a) Optical image of $In_{0.85}Ga_{0.15}As$ NWs on Si(111) wafer with a penny as reference. The rainbow color on surface is a result of slight variation of NW density across the wafer. (b) Sideview SEM image of $In_{0.85}Ga_{0.15}As$ NW array and the scale bar represents 1 μm. (c−f) The 45° tilted SEM images of InAs, $In_{0.85}Ga_{0.15}As$, $In_{0.30}Ga_{0.70}As$, and $In_{0.20}Ga_{0.80}As$ NWs, respectively, with same magnification (20 K) and scale bar of 1 μm. Inset in panel e is a high-magnification top view SEM image and the scale bar represents 200 nm. (g) Average diameter and density of $In_xGa_{1-x}As$ NWs on Si(111) substrate as a function of In composition, x, at growth temperature of 570 °C. (h) Average diameter of InAs NWs as a function of growth temperature.

ternary NWs.[24−26] In addition, electrically pumped optoelectronic devices that require controllable doping in NWs remain to be explored. In this article, we report the heterogeneous epitaxy of high aspect ratio $In_xGa_{1-x}As$ NW arrays with composition tuning in almost the entire range (x = 0.2−1.0) on (111), (110), and (100) Si substrates, detailed structural analysis as a function of indium (In) composition, as well as demonstration of effective n-$In_xGa_{1-x}As$ NW and p-Si junctions in photovoltaic devices.

Figure 1a shows an optical image of half of a 2 in. Si(111) wafer covered with $In_{0.85}Ga_{0.15}As$ NW array, next to a U.S. penny for size reference. The color dispersion reflects slight variation of the NW density, where the NWs appear in most areas except near some edges. Figure 1b shows the sideview SEM of an $In_{0.85}Ga_{0.15}As$ NW array. We emphasize that there is no catalyst and no patterning present on the substrate before NW growth, and $In_xGa_{1-x}As$ NW self-assembles across the whole Si wafer with density exceeding 1×10^8 cm^{-2}. Figure 1c−f shows SEM images of $In_xGa_{1-x}As$ NWs on Si(111) substrates for four different In compositions as indicated. It has been established that there exists a critical diameter (CD) for epitaxial NWs grown on lattice-mismatched substrates; when nuclei are below the CD, well-aligned coherent NWs can be grown, while above the CD, irregular

dx.doi.org/10.1021/nl202676b |*Nano Lett.* 2011, 11, 4831–4838

structures such as nanoneedles or islands form, as demonstrated for several binary material systems.[27−30] Similar to the critical thickness in 2D heteroepitaxy and self-assembled S−K quantum dots,[31,32] experimentally determined CDs for 1D heteroepitaxy is often much larger than the theoretical values[28] and growth parameters such as temperature, flux rate, and flux ratios can significantly change experimental CDs thus NW yield.[29] The growth temperatures of the $In_xGa_{1-x}As$ NWs shown in Figure 1c−f are 540, 570, 590, and 590 °C, respectively. These temperatures have been optimized separately for each composition to minimize island formation and maximize vertical NW growth on the substrate. The optimum growth temperature has been found to increase as In composition decreases.

Under optimized growth conditions, NWs are vertically grown on Si(111) substrate with no visible tapering, and have a hexagon-shaped cross-section as can be seen in the inset of Figure 1e. This indicates that the nucleation of $In_xGa_{1-x}As$ NWs occurs heterogeneously at silicon(111) surface with hexagonal close packed lattice structure, and subsequent growth prefers homoepitaxy on top of the $In_xGa_{1-x}As$ surface, resulting in vertical NWs with uniform diameter. The nontapered growth allows for the formation of high aspect ratio NWs, which is critically important for NW array-based devices such as solar cells. All NWs possess clear crystal facets, which are presumably (111) top facets surrounded by six $\{1\bar{1}0\}$ side facets.[33] While InAs NWs are definitively straight and vertical (Figure 1c), a portion of the ternary $In_xGa_{1-x}As$ NWs are slightly bent at the top as seen in Figure 1d−f. It has been postulated that InAs NWs are grown vertically on Si(111) substrate while the lattice mismatch strain energy is relieved via the lateral direction.[5,29,30] For the ternary case (i.e., $In_xGa_{1-x}As$), the energy relaxation via lateral direction may not be uniform if composition inhomogeneity exists. We attribute the bending of $In_xGa_{1-x}As$ NWs observed here to phase segregation, which has been observed through transmission electron microscopy (TEM) and X-ray diffraction (XRD) characterization and will be discussed later.

Plotted in Figure 1g is the $In_xGa_{1-x}As$ NW diameter and density as a function of In composition grown at the same temperature with size dispersion indicated by error bars. The diameter of the $In_xGa_{1-x}As$ NWs is inversely proportional to the In composition, while the density changes in the opposite direction. This is consistent with the binary systems[28,29] in terms of lattice mismatch trend and can be understood because lower indium composition corresponds to smaller lattice mismatch with silicon and therefore, larger size and less amount of NW nuclei. NW diameters can also be changed by growth condition. Figure 1h shows that the average diameter for InAs NW increases from 33 to 85 nm as the temperature increases from 520 to 570 °C. The temperature dependence of NW diameter is related to adatom mobility, which increases with substrate temperature and promotes the formation of larger nuclei.[34] It was reported that in the temperature range of 430−470 °C, the maximum diameter was 26 nm for InAs NWs grown on silicon via Au-catalyzed vapor−liquid−solid (VLS) mechanism. The NW diameter in this case is actually independent of the Au catalyst size,[28] implying the importance of critical diameter in 1D heteroepitaxy. For all ternary $In_xGa_{1-x}As$ NWs reported here, the optimum V/III ratio is lower than 50, and it decreases with increasing Ga%. In contrast, the V/III ratio for the growth of InAs nanowires on Si(111) was reported to be in the range of 100−300.[5,7] We believe that under high V/III condition, which facilitates lateral growth,[8] the diameter of $In_xGa_{1-x}As$ nuclei may readily exceed the 1D heteroepitaxy critical diameter thus prevent NW growth.

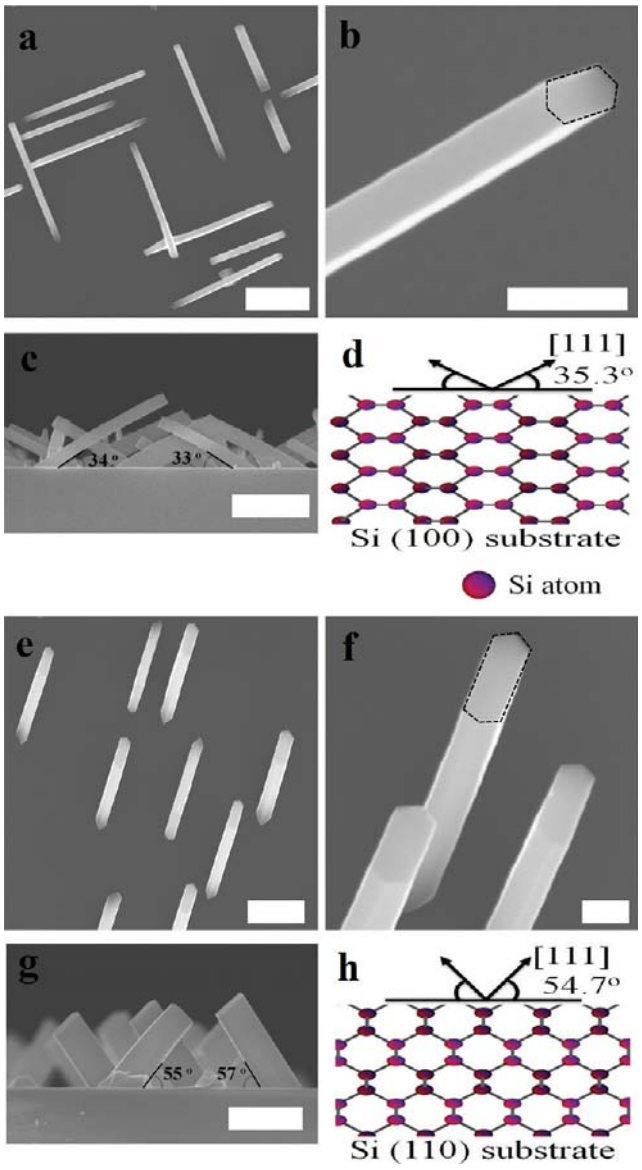

Figure 2. $In_{0.3}Ga_{0.7}As$ NWs grown on non-(111) Si substrates. (a−c) SEM images of NWs grown on Si(100) substrate. (e−g) NWs grown on Si (110) substrate. (d,h) Illustrations of the cross-sectional atomic structure and orientations for Si(100) and (110), respectively. Panels a and e are the top view; b and f are 45 ° tilted view with the top facets outlined; and c and g are sideview. The scale bars in panels a, c, e, and g represent 1 μm while the scale bars in b and f are 200 nm.

Interestingly, the NWs do not grow vertically in the 1D fashion indefinitely. The average height of $In_xGa_{1-x}As$ NWs first scales linearly with growth time, then becomes nearly saturated after a certain height, as shown in Figure S1 in the Supporting Information. The diameter of the NWs starts to increase once the height is saturated, implying the onset of sidewall growth and suppression of vertical growth. The maximum NW height achievable is proportional to the In composition. For example, $In_{0.2}Ga_{0.8}As$ reaches saturation at ~3 μm while height saturation does not occur for InAs NW until >10 μm. The height saturation

dx.doi.org/10.1021/nl202676b |*Nano Lett.* 2011, 11, 4831–4838

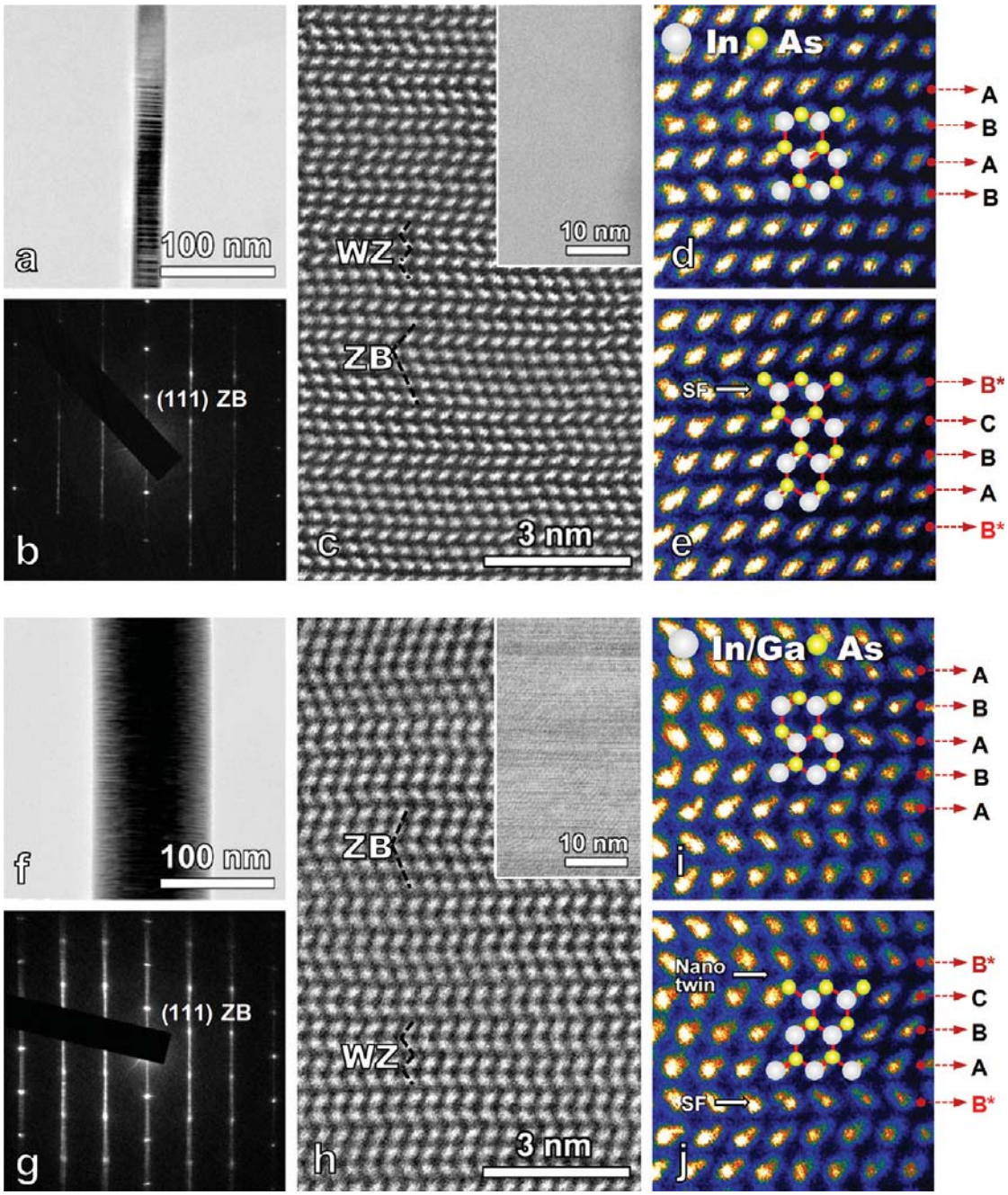

Figure 3. Electron microscopy characterization of $In_xGa_{1-x}As$ NWs. (a−e) InAs NW with a diameter of 30 nm and (f−j) $In_{0.30}Ga_{0.70}As$ with a diameter of 130 nm. Both NW samples show intermixing of WZ (AB* stacking) and ZB (ABC stacking) with ZB dominant in InAs and WZ dominant in $In_{0.30}Ga_{0.70}As$. Nano twins and stacking faults (SF) are indicated in the figures. The Z-contrast STEM image of the inset in panel h for $In_{0.30}Ga_{0.70}As$ NW shows weak contrast modulations suggesting slightly In rich (brighter contrast) and Ga rich (darker contrast) regions, respectively. The atomic structure models are superimposed on the atomic resolution Z-contrast STEM images in panels d, e, i and j. The stacking are labeled with * denoting layers with the In(Ga)-As bonds toward upper left directions. The mixture of WZ and ZB and stacking faults leads to streaky lines in the recorded diffraction patterns in panels b and g and contrast modulations in bright field TEM images in panels a and f.

dependence on In composition could be related to high surface mobility of In compared to Ga, which facilitates more indium diffusion to the 1D growth front. However, no tapering at the NW bottom has been observed before or after height saturation and no systematic composition variation was measured along the axial direction (Figure S2 in Supporting Information). This is in clear contrast to Au catalyzed VLS InGaAs (x = 0.19− 0.23) nanowire growth on GaAs (111)B substrate.[26] Attempt to extend the NW length by switching to a higher In composition before saturation is reached, resulted in growth on the NW sidewall instead of continued 1D epitaxy. Although detailed mechanism for the height saturation is not clear at this point, mismatch strain and related surface and interfacial free-energy, as well as surface diffusion, undoubtedly play important roles.

dx.doi.org/10.1021/nl202676b |*Nano Lett.* 2011, 11, 4831–4838

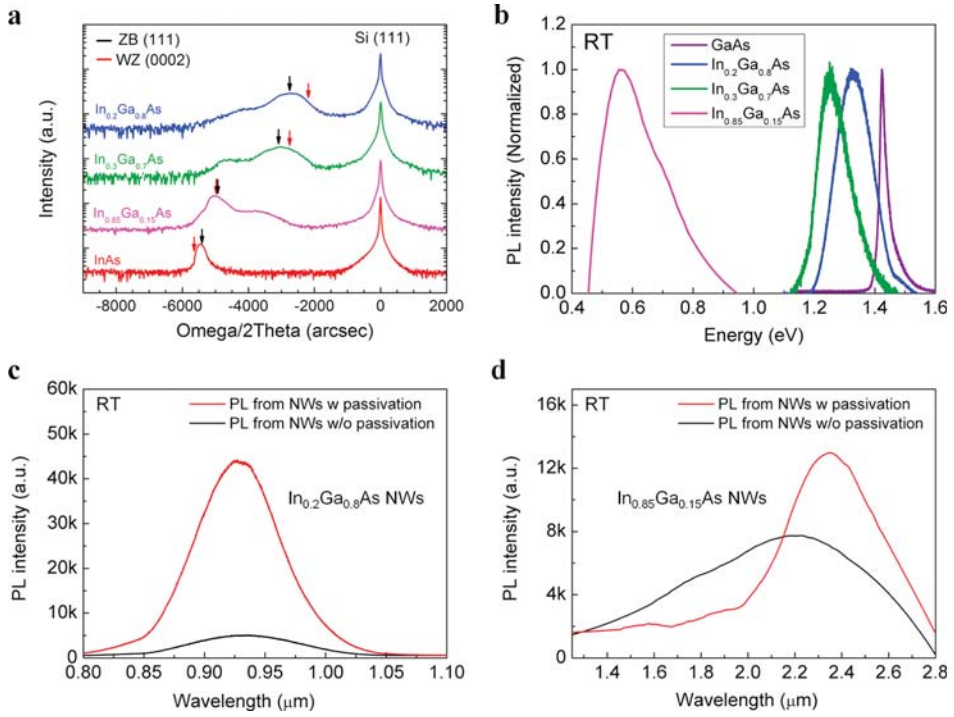

Figure 4. X-ray diffraction and PL spectra of $In_xGa_{1-x}As$ NWs on Si(111) substrate. (a) Each XRD spectrum shows the Si substrate peak, along with the epitaxial $In_xGa_{1-x}As$ peaks to the left on a log intensity scale. (b) Room-temperature micro-PL spectra from $In_{0.85}Ga_{0.15}As$, $In_{0.3}Ga_{0.7}As$, and $In_{0.2}Ga_{0.8}As$ NW array on Si(111) substrates, along with a semi-insulating GaAs bulk substrate as reference. Intensity is normalized. (c,d) Room-temperature micro-PL for $In_{0.2}Ga_{0.8}As$ NW array and $In_{0.85}Ga_{0.15}As$ NW array before and after GaAs passivation.

To further understand the heteroepitaxial growth mechanism of NWs, we have also grown $In_xGa_{1-x}As$ nanowires on Si substrates with different orientations. Figure 2 shows the SEM images of $In_{0.3}Ga_{0.7}As$ NWs grown on Si(100) and (110) substrates, along with illustrations of the atomic structure and orientations of the Si substrates. On Si(100) substrate, the $In_{0.3}Ga_{0.7}As$ NWs are oriented ~34° off the (100) plane (Figure 2c), which corresponds to the ⟨111⟩ direction (Figure 2d). The top view image (Figure 2a) reveals perpendicular sets of NWs, indicating that all four of the ⟨111⟩ orientations exist. Similarly, the $In_{0.3}Ga_{0.7}As$ NWs grown on Si (110) substrate extend along the ⟨111⟩ direction that is angled from the (110) plane by 54.7° as seen in Figure 2g. Since there are only two available ⟨111⟩ directions on (110) substrate,[35,36] no perpendicular set is observed. Figure 2b,f show the tilted view of the ⟨111⟩ $In_{0.3}Ga_{0.7}As$ NWs grown on Si(100) and (110) substrates, respectively, showing the top facets in irregular hexagon shapes with two parallel elongated edges. This is in contrast to the NWs grown on Si(111) substrates where the top facets appear as regular hexagons (see inset in Figure 1e). Our observation of the persistence of ⟨111⟩ growth direction irrespective of substrate orientation for the catalyst-free 1D heteroepitaxy confirms that ⟨111⟩ is the most energetically favorable direction with and without catalyst for homo or heteroepitaxy of NWs, except under kinetically controlled conditions.[36]

The growth of NW along ⟨111⟩ direction frequently yields twinning and stacking faults in compound semiconductors.[1,6,35,37] Shown in Figure 3 are (S)TEM images and electron diffraction patterns of InAs and $In_{0.30}Ga_{0.70}As$ NWs. All images clearly show ordered crystalline planes which correspond to a mixture of zinc-blende (ZB) and wurtzite (WZ) structures often alternating every few monolayers. The existence of massive stacking faults can also be seen from the streaky lines in the electron patterns (Figure 3b,g) recorded from individual NWs using a 100 nm-sized electron beam.[38] $In_{0.3}Ga_{0.70}As$ appears to show stronger streaky lines than InAs, especially for the center row including the direct beam. Remarkably, no misfit dislocation has been observed through the entire observed NW length and for all compositions.

The arrangements of WZ and ZB layers can be determined directly from atomic resolution HAADF-STEM images where the atomic models are superimposed directly on the experimental images, as shown in Figure 3d,e and i,j. The preference of WZ or ZB polytype seems to be composition dependent. Careful examination of the atomic plane stacking reveals that ZB components dominate in InAs NW, while more WZ polytype exists in $In_{0.3}Ga_{0.7}As$ NW. This trend characterized by In rich or Ga rich end of the $In_xGa_{1-x}As$ seems to persist systematically with for all the compositions we have examined and is consistent with the binary InAs and GaAs NW cases.[5,39] It is intriguing that stable ZB bulk III−V semiconductor sometimes takes on WZ structures in epitaxially grown NWs of the same material, and our observation of the composition dependence may shine light on the fundamental mechanism.

In addition to phase intermixing between WZ and ZB, composition inhomogeneity has been observed in the ternary $In_xGa_{1-x}As$ NWs, as evidenced by the Z-contrast HRTEM images of $In_{0.3}Ga_{0.7}As$ in Figure 3h inset, where darker contrast bands normal to the [111] direction corresponds to the Ga rich region. Notice that the dark bands are absent in InAs NWs (Figure 3c inset). The phase separation for the ternary NWs has also been observed in XRD spectra, as will be discussed below.

dx.doi.org/10.1021/nl202676b |*Nano Lett.* 2011, 11, 4831–4838

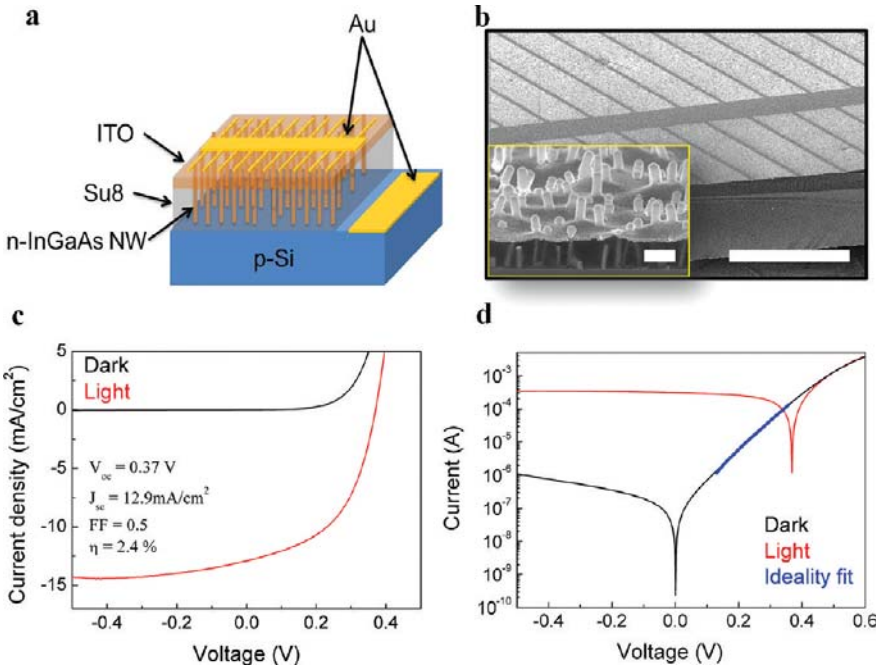

Figure 5. Photovoltaic device with an n-$In_{0.3}Ga_{0.7}As$ NW array (sidewalls passivated with n^+-GaAs) on a p-Si(111) substrate. (a) Schematic illustration of a fully fabricated photovoltaic device using n-type InGaAs NWs grown on a p-type Si substrate. (b) SEM image of device cross section with inset showing the protruded InGaAs NWs above the transparent SU-8 filling. The scale bars in panel b and inset of b represent 500 and 1 μm, respectively. (c) $I-V$ characteristics of the photovoltaic device in dark and under AM 1.5 spectrum illumination. (d) Semilog plot of the $I-V$ characteristics with ideality factor extracted from the linear region (blue line).

XRD measurements are used to determine composition and evaluate the epitaxial crystal quality. Shown in Figure 4a are XRD rocking curves for various compositions of $In_xGa_{1-x}As$ NWs on Si(111) substrate plotted on a logarithmic scale. The peak at zero arcsec is assigned to the Si(111) substrate which corresponds to 28.4° in 2-θ. Other peaks appearing at −5400, −4914, −3114, and −2754 arcsec correspond to the ZB form of InAs, $In_{0.85}Ga_{0.15}As$, $In_{0.3}Ga_{0.7}As$, and $In_{0.2}Ga_{0.8}As$, respectively, when 100% relaxation is assumed. The relationship between the X-ray determined solid state composition and molar ratio of gas phase group III precursors is summarized in Table S1 in the Supporting Information. The XRD spectra confirms the direct epitaxial relationship between Si and $In_xGa_{1-x}As$ NWs (i.e., $In_xGa_{1-x}As$-[111]||Si [111]). The binary InAs NWs show a relatively sharp single peak. In contrast, the ternary $In_xGa_{1-x}As$ NWs show two peaks convoluted into one broad peak with a clear shoulder either on the In or Ga rich side. We attribute the additional peak to the segregation of In and Ga atoms during NW growth, consistent with the phase separation observed in the Z-contrast STEM images above. Notably, the amount of phase separation appear to decrease as Ga composition increases, as suggested by the intensity of the shoulder peaks. As indicated by the corresponding arrows in Figure 4a, the WZ (0002) and ZB (111) peaks of $In_xGa_{1-x}As$, deduced from the lattice constants of GaAs and InAs using Vegard's law,[40,41] are too close to be clearly distinguished from each other when the peaks are as broad as they are. However, it is safe to infer from the XRD spectra of $x = 0.2$ and 0.3 that both WZ and ZB phases coexist in the $In_xGa_{1-x}As$ NWs.

We have also measured the photoluminescence (PL) spectra of the $In_xGa_{1-x}As$ (x = 0.2, 0.3, and 0.85) NW arrays and compared to that of GaAs bulk substrate, as shown in Figure 4b. A single broad peak is observed readily at room temperature for all samples without sidewall passivation. The PL peak for the $In_{0.85}Ga_{0.15}As$ NW array is broader compared to those for the $In_{0.3}Ga_{0.7}As$ and $In_{0.2}Ga_{0.8}As$ NW arrays, indicating a larger distribution of composition in such sample, probably as a result of indium diffusion during growth and cool down. Passivating these $In_xGa_{1-x}As$ NWs with a GaAs shell, which is necessary to reduce surface recombination for device applications, enhances the intensity and reduces the peak width, as shown in Figure 4c,d. The intensity enhancement is more pronounced for Ga rich NWs because of the higher carrier recombination rate of GaAs, while peak width change is more significant for the In rich NWs because of the higher mobility of In. The peak positions of $In_{0.85}Ga_{0.15}As$, $In_{0.3}Ga_{0.7}As$, and $In_{0.2}Ga_{0.8}As$ NWs are 0.56, 1.25, and 1.33 eV, respectively. When compared to their ZB bulk structures,[42] these peaks are 100−200 meV higher, with more blue shift for higher Ga composition. Because of the large diameters of these NWs, quantum confinement cannot be responsible for the blue shift. We believe this is related to the existence of WZ phase in the NWs for these compositions,[43] consistent with the TEM results above. Similar blue shift has been reported in InP NWs and was attributed to the WZ phase.[44] We note that the magnitude of the blue shift observed is larger than expected from bandgap difference between WZ and ZB phases in bulk $In_xGa_{1-x}As$ of the same composition. However, this could be due to the uncertainty in composition assignment of the NWs from XRD spectra where $In_xGa_{1-x}As$ is assumed to be 100% relaxed. For example, adding 3% of residual compressive strain in the XRD simulation would lead to a complete match to the bulk ZB and WZ bandgap difference for $In_{0.3}Ga_{0.7}As$.

$In_xGa_{1-x}As$ NWs directly grown on Si substrates can be used for various practical devices such as LEDs in the near-infrared

dx.doi.org/10.1021/nl202676b |*Nano Lett.* 2011, 11, 4831–4838

wavelength range as well as multijunction solar cells. The prospect of having a continuously tunable semiconductor material system on the same substrate that can match different parts of the solar spectrum for maximum absorption is highly desirable. One-dimensional heteroepitaxy of $In_xGa_{1-x}As$ NWs on Si in almost the entire composition range developed here makes continuous bandgap engineering from ~0.36−1.4 eV on the same platform a reality. In addition, the high aspect ratio NW matrix enhances light trapping by decreasing light reflection (Figure S3 in Supporting Information) and the direct bandgap increases absorption efficiency.[45−47] To test the electrical characteristics of $In_xGa_{1-x}As$ NWs and their heterogeneous interface with the Si substrate, photovoltaic devices consisting of n-type $In_{0.3}Ga_{0.7}As$ NW array on a p-type Si substrate are fabricated. Schematic illustration of a fully fabricated solar cell is illustrated in Figure 5a. Sideview SEM images of a fully fabricated solar cell device are shown in Figure 5b. The NWs were not intentionally doped but their background appears n-type as is the case for bulk $In_xGa_{1-x}As$ materials. The $In_{0.3}Ga_{0.7}As$ NWs have been passivated to reduce surface recombination[48] by a GaAs layer in situ, which is heavily doped using disilane (Si_2H_6) source to serve as n^+ contact.[49] Figure 5c shows the $I-V$ characteristics of the photovoltaic device in dark and under air mass 1.5 (AM 1. 5, 100 mW/cm^2) solar simulator at room temperature. The current−voltage ($I-V$) curve under dark condition shows a rectification ratio larger than 10^3 at ±0.7 V and very low reverse leakage current density (e.g., 2×10^{-3} mA at −0.7 V). This verifies that high quality p−n junction is formed between n-type $In_{0.3}Ga_{0.7}As$ NW array and p-type Si substrate, despite the significant lattice mismatch. V_{oc}, I_{sc}, and fill factor (FF) are 0.37 V, 12.9 mA/cm^2, and 0.5, respectively. Ideality factor of the p−n diode extracted from the linear portion of the $\ln(I)-V$ plot shown in Figure 5d is 1.9. Note that fill factor of 0.5 is very low compared to the calculated value from empirical equation in standard solar cells,[50] probably due to the high parasitic resistance from poor quality ITO. The series resistance of the photovoltaic device calculated is 6 Ω cm^2. Despite of that, the operating voltage and efficiency are higher by nearly 4 times compared to the PV device using InAs NWs on Si substrate.[5] This can be attributed to the better overlap of $In_{0.3}Ga_{0.7}As$ bandgap with the solar spectrum,[51] underling the importance of bandgap engineering of NWs. The energy conversion efficiency is calculated to be 2.4%, even though the $In_{0.3}Ga_{0.7}As$ NW area coverage is only ~2.2% and the height is ~5 μm. In comparison, the state of the art bottom-up grown Si NW array solar cell has an efficiency of 3.81% with a geometrical coverage that is 5× larger (i.e., 10%).[52] We attribute this to the ~10× improvement in absorption coefficient of $In_{0.3}Ga_{0.7}As$ over Si as a result of the direct bandgap.[51] The energy conversion efficiency of the $In_{0.3}Ga_{0.7}As$ NW array can be further enhanced by using advanced technique for light absorption (e.g., incorporating Al_2O_3 dielectric particles that scatter light incident among wires[52]) and optimized transparent and metal contacts.

In conclusion, we have demonstrated 1D heteroepitaxial $In_xGa_{1-x}As$ growth on Si substrates without any catalyst and pattern assistance over almost the entire composition range across 2 in. wafers. Structural analysis of the NW structures reveals no dislocations, but WZ and ZB polytypic phase transition that is composition dependent. Despite of the massive stacking faults, the fabricated photovoltaic device shows good p−n junction characteristics between the $In_xGa_{1-x}As$ NW array and Si substrate. Tandem cells consisting of a NW subcell monolithically grown on top (or bottom, depending on the bandgap energy relative to Si) of a planar Si p−n junction subcell, can be envisioned. The same 1D heteroepitaxy principle could be applied to other material systems such as III−V on Ge substrates, enabling better bandgap matching for multijunction solar cells. NW based tandem cells allow the use of simpler epitaxial structures (e.g., without sophisticated graded metamorphic junctions in conventional tandem cells), which should lead to better reliability and cost saving. The establishment of a tunable, and scalable III−V 1D heteroepitaxy method could also enable applications including optoelectronic communications, gas sensing, and near-infrared LEDs.

Methods. The InGaAs nanowires (NWs) were grown by low pressure metal organic chemical vapor deposition (MOCVD) using an Aixtron horizontal reactor. p-type Si ⟨111⟩ wafers (0.15−0.25 Ω-cm, Crysteco Inc.) were used as substrates. The substrates were etched using buffered-HF (Transene, Inc.) to remove the native oxide and then rinsed in deionized water for about 5 s and dried with N_2. The substrates were then immediately loaded into the MOCVD chamber and heated to growth temperature under H_2 carrier gas. Trimethylindium [$(CH_3)_3In$, TMIn] and trimethylgallium [$(CH_3)_3Ga$, TMGa] were used as Ga and In precursors, respectively. AsH_3 was used as group-V source. After the reactor reached growth temperature, AsH_3, TMGa, and TMIn were simultaneously switched into the reactor. The flow rate of H_2 carrier gas was maintained at 15 L/min during the entire growth. The molar flows of TMIn and TMGa were varied in the range of 1.3×10^{-5}−4.5×10^{-6} and 1.8×10^{-5}−7.6×10^{-6} (mols/min), respectively. The nominal V/III ratio was in the range of 20−100. The morphologies of $In_xGa_{1-x}As$ NWs were characterized by scanning electron microscopy (SEM, Hitachi-S4800). The XRD spectra were measured using Philips X'pert system (PANalytical inc.). The indium composition for all growths was determined from the XRD rocking curves assuming complete relaxation. The room temperature (RT) PL was measured using micro PL system with a Si CCD detector and 633 nm He−Ne laser for $In_xGa_{1-x}As$ (x = 0.2 and 0.3) NW samples, and a Ti:Sapphire laser at 800 nm with an InSb detector for $In_xGa_{1-x}As$ (x = 0.85) NW sample. The TEM images were measured using JEOL 2010 Cryo TEM.

For solar cell structures, $In_xGa_{1-x}As$ NWs were first grown on Si substrate, then a GaAs shell was grown in situ at higher temperature to passivate the NW surface. The uniform GaAs sidewall passivation was confirmed by dipping the NWs in a selective GaAs etchant (i.e., citric acid:H_2O_2) and exposing the $In_xGa_{1-x}As$ core (Supporting Information Figure S4). SU8 is filled inbetween NWs with the NW tips exposed for contact. Indium tin oxide (100−200 nm thick) was subsequently deposited, followed by gold finger electrodes on top of ITO pad and astripe contact on the Si substrate. Detailed fabrication sequence can be found in Supporting Information Figure S6.

■ ASSOCIATED CONTENT

Supporting Information. Additional information, figures, and table. This material is available free of charge via the Internet at http://pubs.acs.org.

■ AUTHOR INFORMATION

Corresponding Author
*E-mail: xiuling@illinois.edu.

■ ACKNOWLEDGMENT

The authors would like to acknowledge Professor Ralph Nuzzo for allowing us access to the solar simulator and technical discussions with Xin Miao, Ryan Dowdy, and Chen Zhang. Financial support was provided in part by DOE Division of Materials Sciences under Award Numbers DEFG02-01ER45923 and DE-FG02-07ER46471 through the Frederick Seitz Materials Research Laboratory at the University of Illinois at Urbana-Champaign; NSF STC under Award Number 0749028 (CMMI); and NSF DMR under Award Number 1006581. TEM work was carried out in the Frederick Seitz Materials Research Laboratory Central Facilities, University of Illinois, which are partially supported by the U.S. Department of Energy under grants DE-FG02-07ER46453 and DE-FG02-07ER46471.

■ REFERENCES

(1) Martensson, T.; Svensson, C. P. T.; Wacaser, B. A.; Larsson, M. W.; Seifert, W.; Deppert, K.; Gustafsson, A.; Wallenberg, L. R.; Samuelson, L. *Nano Lett.* **2004**, *4* (10), 1987–1990.

(2) Tomioka, K.; Motohisa, J.; Hara, S.; Hiruma, K.; Fukui, T. *Nano Lett.* **2010**, *10* (5), 1639–1644.

(3) Mandl, B.; Stangl, J.; Martensson, T.; Mikkelsen, A.; Eriksson, J.; Karlsson, L. S.; Bauer, G.; Samuelson, L.; Seifert, W. *Nano Lett.* **2006**, *6* (8), 1817–1821.

(4) Chuang, L. C.; Kar Wei, N.; Tran, T. T. D.; Wai Son, K.; Moewe, M.; Crankshaw, S.; Chen, R.; Chang-Hasnain, C. In *Single Crystalline GaAs Nanoneedles Grown on 46% Lattice-Mismatched Sapphire with Bright Luminescence*; 2010, IEEE: Piscataway, NJ; p 2.

(5) Wei, W.; Bao, X.-Y.; Soci, C.; Ding, Y.; Wang, Z.-L.; Wang, D. *Nano Lett.* **2009**, *9* (8), 2926–2934.

(6) Mårtensson, T.; Wagner, J. B.; Hilner, E.; Mikkelsen, A.; Thelander, C.; Stangl, J.; Ohlsson, B. J.; Gustafsson, A.; Lundgren, E.; Samuelson, L.; Seifert, W. *Adv. Mater.* **2007**, *19* (14), 1801–1806.

(7) Tomioka, K.; Motohisa, J.; Hara, S.; Fukui, T. *Nano Lett.* **2008**, *8* (10), 3475–3480.

(8) Dayeh, S. A.; Yu, E. T.; Wang, D. *Nano Lett.* **2007**, *7* (8), 2486–2490.

(9) Bakkers, E. P. A. M.; van Dam, J. A.; De Franceschi, S.; Kouwenhoven, L. P.; Kaiser, M.; Verheijen, M.; Wondergem, H.; van der Sluis, P. *Nat. Mater.* **2004**, *3* (11), 769–773.

(10) Allen, J. E.; Hemesath, E. R.; Perea, D. E.; Lensch-Falk, J. L.; LiZ., Y; Yin, F.; Gass, M. H.; Wang, P.; Bleloch, A. L.; Palmer, R. E.; Lauhon, L. J. *Nat. Nanotechnol.* **2008**, *3* (3), 168–173.

(11) Perea, D. E.; Allen, J. E.; May, S. J.; Wessels, B. W.; Seidman, D. N.; Lauhon, L. J. *Nano Lett.* **2005**, *6* (2), 181–185.

(12) Sun, M. H.; Leong, E. S. P.; Chin, A. H.; Ning, C. Z.; Cirlin, G. E.; Samsonenko, Y. B.; Dubrovskii, V. G.; Chuang, L.; Chang-Hasnain, C. *Nanotechnology* **2010**, *21* (33), 335705–335705.

(13) Koblmuller, G.; Hertenberger, S.; Vizbaras, K.; Bichler, M.; Bao, F.; Zhang, J.-P.; Abstreiter, G. *Nanotechnology* **2010**, *21* (36), 365602–365602.

(14) Hertenberger, S.; Rudolph, D.; Bichler, M.; Finley, J. J.; Abstreiter, G.; Koblmuller, G. *J. Appl. Phys.* **2010**, *108* (11), 114316.

(15) Johansson, J.; Karlsson, L. S.; Patrik, T.; Svensson, C.; Martensson, T.; Wacaser, B. A.; Deppert, K.; Samuelson, L.; Seifert, W. *Nat. Mater.* **2006**, *5* (7), 574–580.

(16) Rehnstedt, C.; Martensson, T.; Thelander, C.; Samuelson, L.; Wernersson, L.-E.; Ericsson AB, L. *IEEE Trans. Electron Devices* **2008**, *55* (11), 3037–3041.

(17) Offermans, P.; Crego-Calama, M.; Brongersma, S. H. *Nano Lett.* **2010**, *10* (7), 2412–2415.

(18) Capasso, F.; Cho, A. Y. *Surf. Sci.* **1994**, *299−300*, 878–891.

(19) Edman, C. F.; Swint, R. B.; Gurtner, C.; Formosa, R. E.; Roh, S. D.; Lee, K. E.; Swanson, P. D.; Ackley, D. E.; Coleman, J. J.; Heller, M. J. *IEEE Photonics Technol. Lett.* **2000**, *12* (9), 1198–200.

(20) Tchernycheva, M.; Cirlin, G. E.; Patriarche, G.; Travers, L.; Zwiller, V.; Perinetti, U.; Harmand, J.-C. *Nano Lett.* **2007**, *7* (6), 1500–1504.

(21) Shapiro, J. N.; Lin, A.; Wong, P. S.; Scofield, A. C.; Tu, C.; Senanayake, P. N.; Mariani, G.; Liang, B. L.; Huffaker, D. L. *Appl. Phys. Lett.* **2010**, *97* (24), 243102.

(22) Qian, F.; Li, Y.; Gradecak, S.; Park, H.-G.; Dong, Y.; Ding, Y.; Wang, Z. L.; Lieber, C. M. *Nat. Mater.* **2008**, *7* (9), 701–706.

(23) Kuykendall, T.; Ulrich, P.; Aloni, S.; Yang, P. *Nat. Mater.* **2007**, *6* (12), 951–956.

(24) Chen, R.; Tran, T.-T. D.; Ng, K. W.; Ko, W. S.; Chuang, L. C.; Sedgwick, F. G.; Chang-Hasnain, C. *Nat. Photonics* **2011**, *5*, 170–175.

(25) Moewe, M.; Chuang, L. C.; Crankshaw, S.; Ng, K. W.; Chang-Hasnain, C. *Opt. Express* **2009**, *17* (10), 7831–7836.

(26) Kim, Y.; Joyce, H. J.; Gao, Q.; Tan, H. H.; Jagadish, C.; Paladugu, M.; Zou, J.; Suvorova, A. A. *Nano Letters* **2006**, *6* (4), 599–604.

(27) Eaglesham, D. J.; Cerullo, M. *Phys. Rev. Lett.* **1990**, *64* (16), 1943.

(28) Chuang, L. C.; Moewe, M.; Chase, C.; Kobayashi, N. P.; Chang-Hasnain, C.; Crankshaw, S. *Appl. Phys. Lett.* **2007**, *90* (4), 043115.

(29) Ertekin, E.; Greaney, P. A.; Chrzan, D. C.; Sands, T. D. *J. Appl. Phys.* **2005**, *97* (11), 114325.

(30) Glas, F. *Phys. Rev. B* **2006**, *74* (12), 121302.

(31) Hsu, C. H.; Lee, H. Y.; Hsieh, Y. W.; Stetsko, Y. P.; Tang, M. T.; Liang, K. S.; Yeh, N. T.; Chyi, J. I.; Noh, D. Y. *Physica B* **2003**, *336* (1−2), 98–102.

(32) Kegel, I.; Metzger, T. H.; Lorke, A.; Peisl, J.; Stangl, J.; Bauer, G.; Nordlund, K.; Schoenfeld, W. V.; Petroff, P. M. *Phys. Rev. B* **2001**, *63* (3), 035318.

(33) Zardo, I.; Conesa-Boj, S.; Peiro, F.; Morante, J. R.; Arbiol, J.; Uccelli, E.; Abstreiter, G.; Fontcuberta i Morral, A. *Phys. Rev. B* **2009**, *80* (24), 245324.

(34) Gai, Z.; Howe, J. Y.; Guo, J.; Blom, D. A.; Plummer, E. W.; Shen, J. *Appl. Phys. Lett.* **2005**, *86* (2), 023107.

(35) Fortuna, S. A.; Li, X. L. *Semicond. Sci. Technol.* **2010**, *25* (2), 16.

(36) Fortuna, S. A.; Wen, J. G.; Chun, I. S.; Li, X. L. *Nano Lett.* **2008**, *8* (12), 4421–4427.

(37) Chu, H.-J.; Yeh, T.-W.; Stewart, L.; Dapkus, P. D. *Physica Status Solidi C* **2010**, *7* (10), 2494–2497.

(38) Zuo, J. M.; Gao, M.; Tao, J.; Li, B. Q.; Twesten, R.; Petrov, I. *Microsc. Res. Tech.* **2004**, *64* (5−6), 347–355.

(39) Moewe, M.; Chuang, L. C.; Crankshaw, S.; Chase, C.; Chang-Hasnain, C. *Appl. Phys. Lett.* **2008**, *93* (2), 023116.

(40) Yeh, C.-Y.; Lu, Z. W.; Froyen, S.; Zunger, A. *Phys. Rev. B* **1992**, *46* (16), 10086–10097.

(41) Takahashi, K.; Morizumi, T. *Jpn. J. Appl. Phys.* **1966**, *5* (8), 657–662.

(42) Nahory, R. E.; Pollack, M. A.; Johnston, W. D.; Barns, R. L. *Appl. Phys. Lett.* **1978**, *33* (7), 659–61.

(43) Zanolli, Z.; Fuchs, F.; Furthmüller, J.; Barth, U. v.; Bechstedt, F. *Phys. Rev. B* **2007**, *75* (24), 245121.

(44) Kitauchi, Y.; Kobayashi, Y.; Tomioka, K.; Hara, S.; Hiruma, K.; Fukui, T.; Motohisa, J. *Nano Lett.* **2010**, *10* (5), 1699–1703.

(45) Garnett, E.; Yang, P. *Nano Lett.* **2010**, *10* (3), 1082–1087.

(46) Kelzenberg, M. D.; Boettcher, S. W.; Petykiewicz, J. A.; Turner-Evans, D. B.; Putnam, M. C.; Warren, E. L.; Spurgeon, J. M.; Briggs, R. M.; Lewis, N. S.; Atwater, H. A. *Nat. Mater.* **2010**, *9*(3), 239−244.

(47) Fan, Z.; Kapadia, R.; Leu, P. W.; Zhang, X.; Chueh, Y.-L.; Takei, K.; Yu, K.; Jamshidi, A.; Rathore, A. A.; Ruebusch, D. J.; Wu, M.; Javey, A. *Nano Lett.* **2010**, *10* (10), 3823–3827.

(48) Capasso, F.; Williams, G. F. *J. Electrochem. Soc.* **1982**, *129* (4), 821–824.

(49) Tian, B.; Zheng, X.; Kempa, T. J.; Fang, Y.; Yu, N.; Yu, G.; Huang, J.; Lieber, C. M. *Nature* **2007**, *449* (7164), 885–889.

(50) Green, M. A. *Sol. Cells* **1982**, *7* (3), 337–340.

(51) Henry, C. H. *J. Appl. Phys.* **1980**, *51* (8), 4494–4500.

(52) Putnam, M. C.; Boettcher, S. W.; Kelzenberg, M. D.; Turner-Evans, D. B.; Spurgeon, J. M.; Warren, E. L.; Briggs, R. M.; Lewis, N. S.; Atwater, H. A. *Energy Environ. Sci.* **2010**, *3* (8), 1037–1041.